



Edge–texture feature-based image forgery detection with cross-dataset evaluation

Khurshid Asghar^{1,4} · Xianfang Sun⁴ · Paul L. Rosin⁴ · Mubbashar Saddique² · Muhammad Hussain³ · Zulfiqar Habib²

Received: 19 October 2018 / Revised: 8 August 2019 / Accepted: 28 August 2019

© Springer-Verlag GmbH Germany, part of Springer Nature 2019

Abstract

A digital image is a rich medium of information. The development of user-friendly image editing tools has given rise to the need for image forensics. The existing methods for the investigation of the authenticity of an image perform well on a limited set of images or certain datasets but do not generalize well across different datasets. The challenge of image forensics is to detect the traces of tampering which distorts the texture patterns. A method for image forensics is proposed, which employs discriminative robust local binary patterns for encoding tampering traces and a support vector machine for decision making. In addition, to validate the generalization of the proposed method, a new dataset is developed that consists of historic images, which have been tampered with by professionals. Extensive experiments were conducted using the developed dataset as well as the public domain benchmark datasets; the results demonstrate the robustness and effectiveness of the proposed method for tamper detection and validate its cross-dataset generalization. Based on the experimental results, directions are suggested that can improve dataset collection as well as algorithm evaluation protocols. More broadly, discussion in the community is stimulated regarding the very important, but largely neglected, issue of the capability of image forgery detection algorithms to generalize to new test data.

Keywords Image forensics · Image forgery detection · Copy–move · Splicing · Cross-dataset evaluation

1 Introduction

Zulfiqar Habib
drzhabib@cuilahore.edu.pk

Khurshid Asghar
khasghar@uo.edu.pk

Xianfang Sun
SunX2@cardiff.ac.uk

Paul L. Rosin
rosinpl@cardiff.ac.uk

Mubbashar Saddique
mubbashar.saddique@cuilahore.edu.pk

Muhammad Hussain
mhussain@ksu.edu.sa

Digital images are rich source of information in areas such as forensic science, medical imaging, surveillance, journalism, e-services and social networking. On social media applications such as WhatsApp and Facebook, 1.8 billion images are uploaded daily [1]. It has become much easier to manipulate the content of images due to the availability of powerful image editing tools such as Adobe Photoshop [2] and Corel-DRAW [2]. It is difficult for humans to visually detect such image modifications [2, 3].

Figure 1 shows different ways of image tampering such as shadow removal, inserting fake objects, color filtering, image composition and illumination adjustment. An image may be tampered using the following operations: (i) transferring an object or region from one image to another, or even to the same image, which is the most common type of forgery and encompasses both splicing and copy–move operations, see Fig. 2; (ii) inserting fake objects into an image or manipulating an existing object to change its properties; (iii)

¹ Department of Computer Science, University of Okara, Okara, Pakistan

² Department of Computer Science, COMSATS University Islamabad, Lahore Campus, Lahore, Pakistan

³ Department of Computer Science, King Saud University, Riyadh, Saudi Arabia

⁴ School of Computer Science and Informatics, Cardiff University, Cardiff, UK

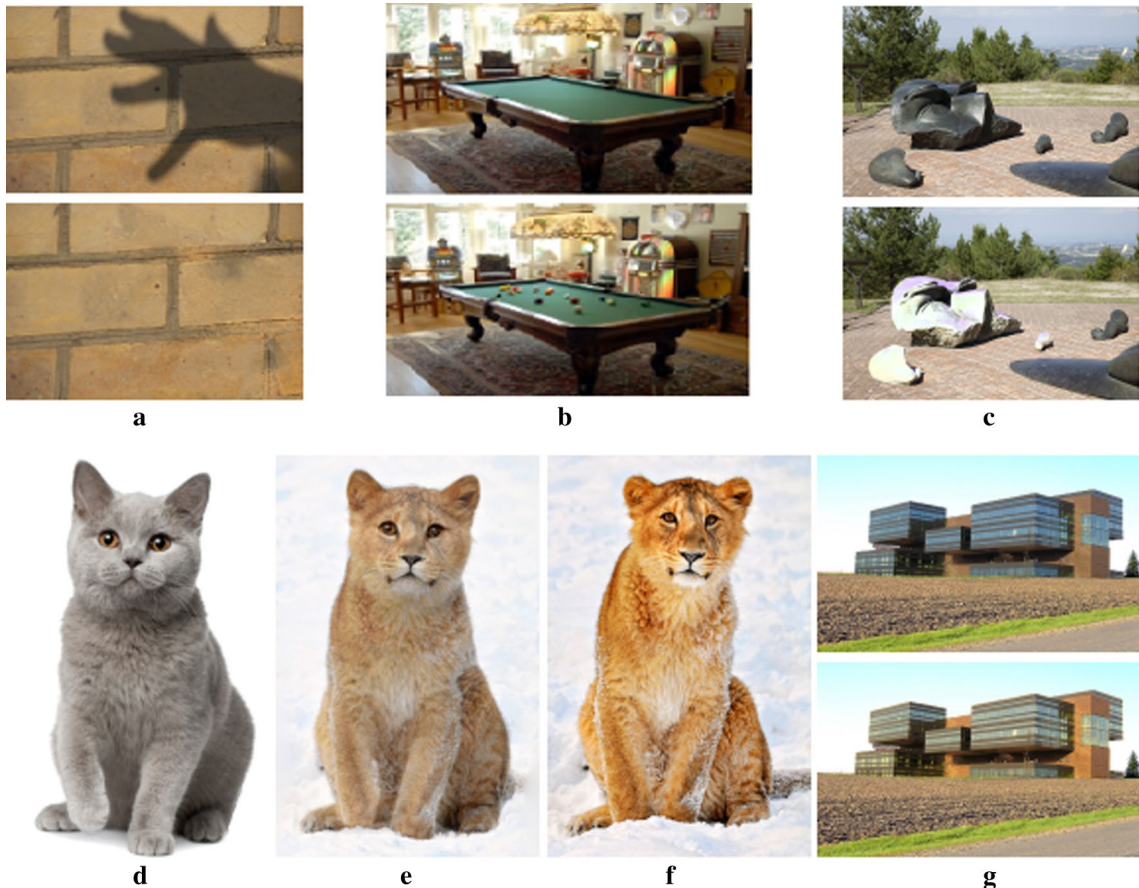


Fig. 1 **a** The hand shadow from the top image has been removed on the bottom image [4]. **b** The balls in the bottom picture are not real, which are inserted using circle objects along with light interactions [5]. **c** The bottom image was filtered to perform color editing on some

of the stone statues [6]. **d–f** The cat in (e) is a composite of the cat in (d) and the leopard in (f) [7]. **g** The building was spliced on the field in the top image, and in the bottom, it had its lighting adjusted to match the composition [8]

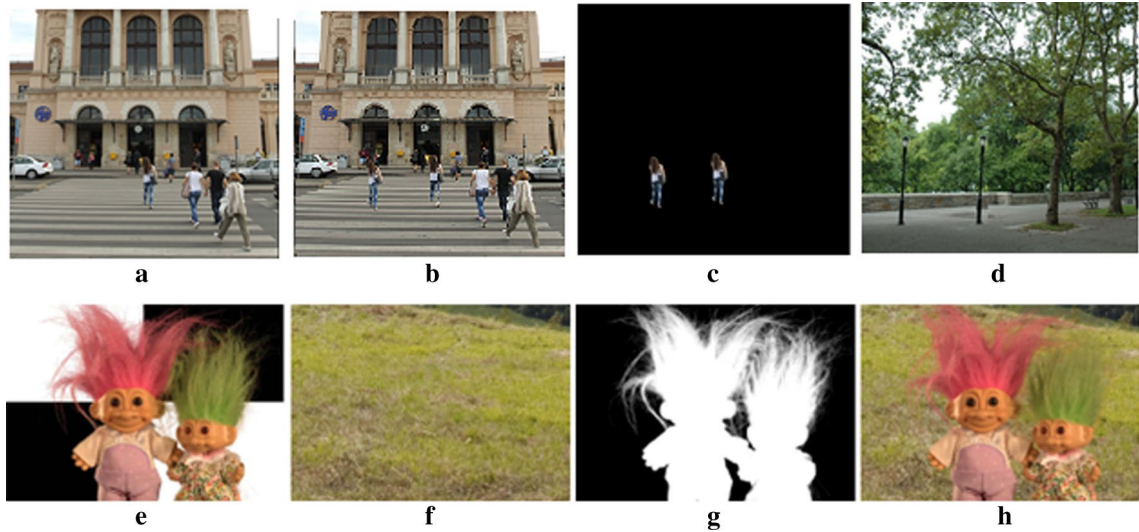


Fig. 2 Examples of copy–move (**a–d**) and splicing (**e–h**) forgeries: **a** Original image [9], **b** tampering is performed by copy and pasting a girl object in the same image to another location [9], **c**

of (**b**), **d** object street lamp is copied to another location in the same image [10], **e** source image [11], **f** target image [11], **g** transference mask of source image, **h** Spliced image

altering image parts related to lights and lighting; and (iv) removing an object or region from the image and hiding it.

Due to an increase in the number of tampered and retouched images, digital contents are nowadays not considered a reliable source of information. It is very difficult to have reliable and efficient image forensic methods, due to the advancement and sophistication in image manipulation operations. Image authentication without using any prior information is called passive or blind approach [2, 12–14] and has received reasonable attention in the literature due to its ability to find forgeries in images by exploiting the traces/artifacts via modeling the artifacts of forgery (discontinuities and inconsistencies in the form of edges, lines and corners) left by the tampering process. These traces act as features for image tampering detection [2, 15, 16].

To construct a simplified and computationally efficient image forgery detection model, we employ discriminative robust local binary patterns (DRLBP) [17], which encode the structural changes that occur in images due to forgery. During model construction, a real forgery example dataset is required to validate the model. For this purpose, a new dataset consisting of historic images that have been tampered by professionals is developed, referred to in this paper as the Forged Real Images Throughout History (FRITH). It is used to validate the developed image authentication process together with other existing image forgery evaluation benchmark datasets.

This work has the following four major contributions.

- First, a new dataset FRITH (see Sect. 4 for details) is developed to evaluate the image forgery detection method on realistic scenarios.
- Second, a robust image forgery detection method based on DRLBP and support vector machine (SVM) is proposed to identify whether a given image is authentic or forged. Extraction of salient features is important for any image forgery detection system. Since the texture and contrast of forged images are different to those of authentic images due to structural changes after forgery, the DRLBP code is computed by assigning a weight factor (w) carrying gradient information to capture edge and texture information together. The contrast is high near the boundary of forged areas in the forged images; therefore, the voted bin value is expected to be high as compared to authentic images, which provides additional information of tampering cues (edges).
- Third, the proposed approach is evaluated on cross-datasets (i.e., training and testing on different datasets) to generalize to new data in real applications.
- Fourth, a thorough evaluation and comparison on a variety of benchmark datasets is performed.

The rest of the paper is organized as follows. Related works on image forgery detection are reviewed in Sect. 2. The detail of the proposed technique is described in Sect. 3. Datasets and evaluation criteria are described in Sect. 4. System parameters are described in Sect. 5. Experimental results are presented, discussed and compared with existing works in Sect. 6. The paper is concluded in Sect. 7.

2 Related work

Over the last two decades, numerous works had been performed to detect different types of forgeries in images. Image forgery detection approaches are divided into active and passive (or blind) categories. Active approaches use detection of embedded watermarks or signatures to ensure the authenticity of images [18–23]. Such approaches are limited, because they are difficult to maintain prior information of such pre-embedded watermarks, signatures and secret keys [20]. Therefore, to detect image forgery without having any prior knowledge is an active research field.

Inspired by the research in [24] for perceiving tampered human speech, Ng and Chang [25] and Ng et al. [26] proposed to detect image forgery by means of phase and magnitude features of images. The Columbia Image Splicing Detection Evaluation (CISD) dataset was used for evaluation [27]. The detection accuracy was only 72%, due to differences in the frequency characteristics between audio signals and digital images. High-order wavelet features were passed to an SVM classifier for image forgery detection in [26], and they achieved 80.15% accuracy. Wang et al. [28] detected image forgery using the gray-level co-occurrence matrix (GLCM) of the YCbCr image. The CASIA v1.0 dataset was used for evaluation. The achieved accuracy was 90.5% on the Cr channel. Subsequently, Wang et al. [29] extracted transition probability features from the Cb channel, achieving an accuracy of 95.6% on a subset of the CASIA v2.0 dataset.

A technique based on the modified run-length run-number (RLRN) was proposed by Zhao et al. [30]. He used chrominance components for feature extraction and achieved 94% detection rate. Muhammad et al. [31] decomposed Cb and Cr components using the steerable pyramid transform (SPT) into sub-bands and extracted features using local binary patterns (LBP) from these sub-bands. Significant features were selected and then passed to an SVM for classification. The Columbia Color DVMM, CASIA v1.0 and CASIA v2.0 datasets were used for experiments. The best accuracies reported were 94.8% on CASIA v1.0 dataset, 97.33% on CASIA v2.0 dataset and 96.39% on Columbia Color DVMM dataset. Cozzolino et al. [32] used dense features and achieved 95.92% and 94.61% detection accuracy on FAU and GRIP datasets, respectively. The datasets

contain 48 and 80 authentic and copy-move forged images, respectively.

Rota et al. [33] proposed a blind deep learning approach based on convolutional neural networks (CNN) for tampered image classification. They used the CAISA v2.0 dataset for experiments and achieved 97.44% detection rate.

Hussain et al. [34] evaluated image forgery detection using Weber local descriptor (WLD) and LBP. The tampering traces were computed from chrominance components using WLD and encoded as features using binary patterns. SVM was employed for classification. The method was evaluated on DVMM, CASIA v1.0 and CASIA v2.0 datasets. The impact of WLD and LBP to model tampering traces was thoroughly explored. The performance of the method was reasonable.

Cattaneo et al. [35] performed an experimental analysis of image forgery detection and used the approach of Lin et al. [36] for JPEG tampered image detection. For tampering detection, the authors in [35] estimated the image luminance quality factor and relative frequency of tampered blocks in both authentic and forged images in the CASIA v2.0 dataset and found that the images of the CASIA v2.0 dataset contain some statistical artifacts which can help the detection process. To confirm this, they first used the CASIA v2.0 dataset to evaluate the performance of Lin et al.'s algorithm. According to their experiments, the considered algorithm performs very well on the CASIA v2.0 dataset. Some variants of the original algorithm were then specifically tuned according to the characteristics of the CASIA v2.0 dataset. These variants performed better than their original counterpart. Then, a new unbiased dataset UNISA [35] was assembled and a new set of experiments was carried out on these images. The results showed that the performance of the algorithm and its variants substantially decreased, proving that the algorithm tuned on CASIA v2.0 is not robust.

Pham et al. used Markov features in DCT domain to identify whether a given image is authentic or forged. SVM was used for classification [37]. Experiments were performed using CASIA v1.0 and CASIA v2.0 datasets and achieved 96.90% detection accuracy. The method is evaluated on limited datasets and focused only splicing forgery.

Wang and Kamata [38] proposed mass filter banks using fast Fourier transformation. The features were then fed to ResNet [39], to classify whether an image is tampered or authentic. Yan et al. [40] proposed a method based on deep learning using CNN architecture. The model is trained on recolored and natural images. The method achieved 83.98% detection accuracy and was evaluated on a variety of recolored and natural images. However, evaluation is not performed on forgeries such as copy-move and splicing.

Review of existing image forgery detection techniques shows that encoding structural changes occurred in images because forgery is still a challenge. The success of an image

forgery detection method relies upon how it copes with the structural changes in forged images. In our experiments, we explored LBP, WLD and DRLBP texture descriptors and found that DRLBP models these structural changes well. A variety of benchmark datasets are used for evaluation in our experimental analysis. To ensure the robustness (i.e., the ability to authenticate images in general) of the proposed algorithm, a cross-dataset protocol is adopted, i.e., training and testing are performed on different datasets that have been collected independently.

3 Proposed image forgery detection system

The architectural diagram of the proposed approach is shown in Fig. 3. The system is composed of four major components, i.e., (i) preprocessing, (ii) feature extraction, (iii) classification model building and (iv) testing, using the trained model with cross-dataset validation. The model is trained using an SVM classifier on a set of images (see model training component of Fig. 3), and then, the trained model is used to test/recognize (see testing component of Fig. 3) unseen authentic and forged images.

3.1 Preprocessing

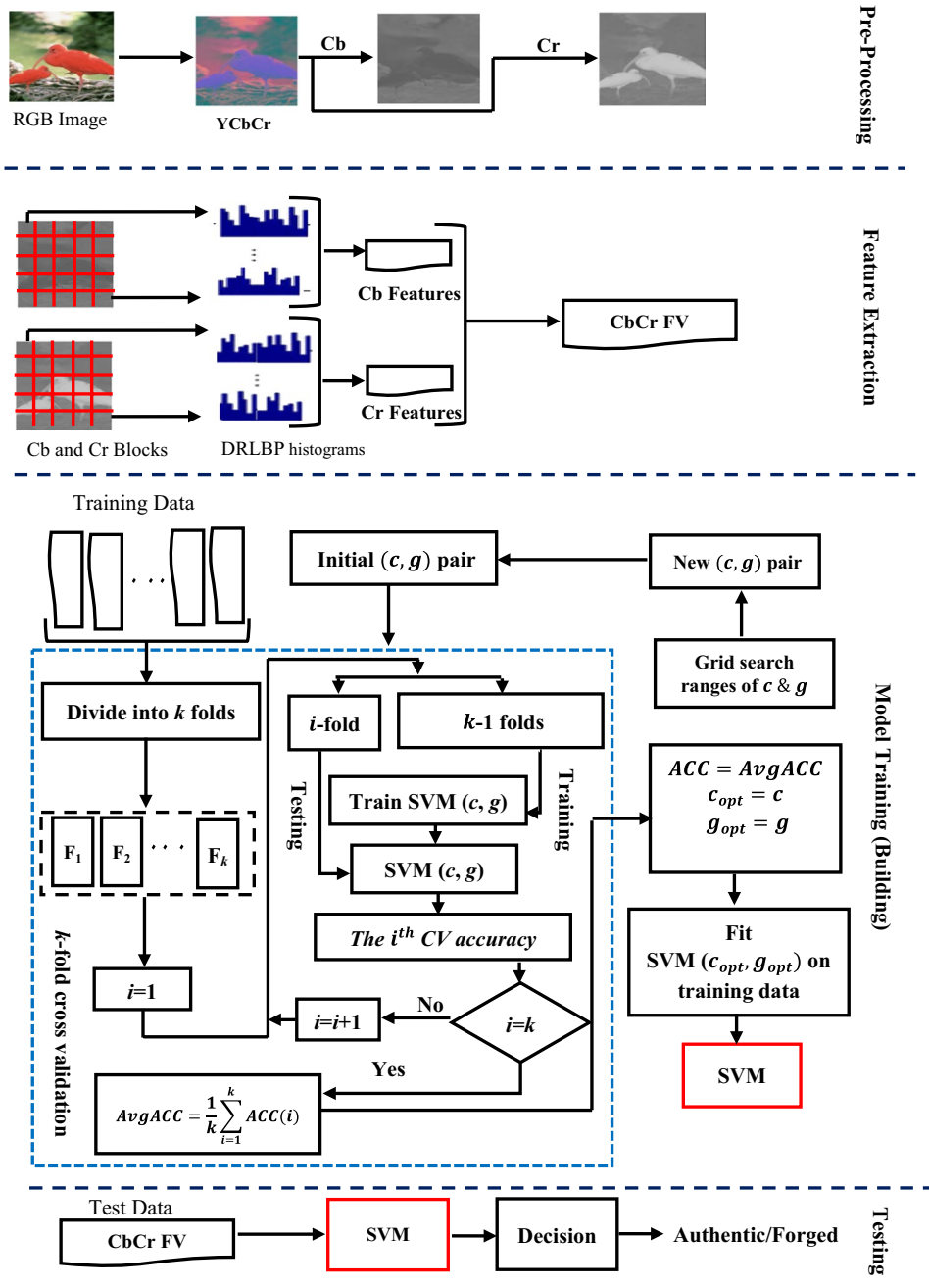
Tampering traces are embedded in the form of edge irregularities [41]. Before feature extraction, it is important to select an appropriate color space. A tampered image is shown in respective components of RGB, HSV and YCbCr color spaces in Fig. 4. It is observed that all components describe the image content in detail except chroma components (CbCr), which emphasize the weak signal content (little image detail) of the image. In general, the content of an image is too strong to hide the tampering traces. Edge irregularities caused by tampering can be noticed in chroma components [41]; therefore, this study uses the YCbCr color space.

After careful visual inspection of the bird's contour in the Y, Cb and Cr components (see Fig. 4), it is found that plenty of image detail covers up the forgery introduced by edges in the Y component, while in Cb (or Cr) component the bird's contour presenting the forged region is sharper than other parts of the image because Cb (or Cr) has little image content as compared to Y (see Fig. 4). Therefore, CbCr components are considered instead of Y component for features extraction.

3.2 Feature extraction

During forgery, edges irregularities are embedded, which disturb the texture of images. Since significant difference is present in the texture of authentic and forged images in the

Fig. 3 Proposed architecture of image forgery detection system



form of small variations, the key question is how to model these small variations. LBP encodes the microstructure patterns [31], but does not capture well the orientation and edge information due to ignorance of small pixel fluctuation and sensitivity to noise. To classify whether an image is authentic or forged, microstructure patterns are required to be encoded with the strength of orientation and edge information. The new DRLBP texture descriptor better represents the microstructure patterns by assigning a weight factor (w) carrying the gradient and texture information together. In this way, DRLBP captures edge irregularities and local

changes by encoding the edge and texture information together. Due to this reason, DRLBP is used in this study.

To explain how these changes are modeled, an example of image forgery is explained (see Fig. 5). In Fig. 5a, the white box region is copied and pasted into the black box region. The zoomed-in view of the black box region after forgery in Fig. 5c shows that the texture of the black box region after forgery is disturbed and artifacts of tampering (edges, lines and corners) are introduced. To hide these artifacts, the forged image is post-processed using blurring (see Fig. 5d). The zoomed-in versions of the black box

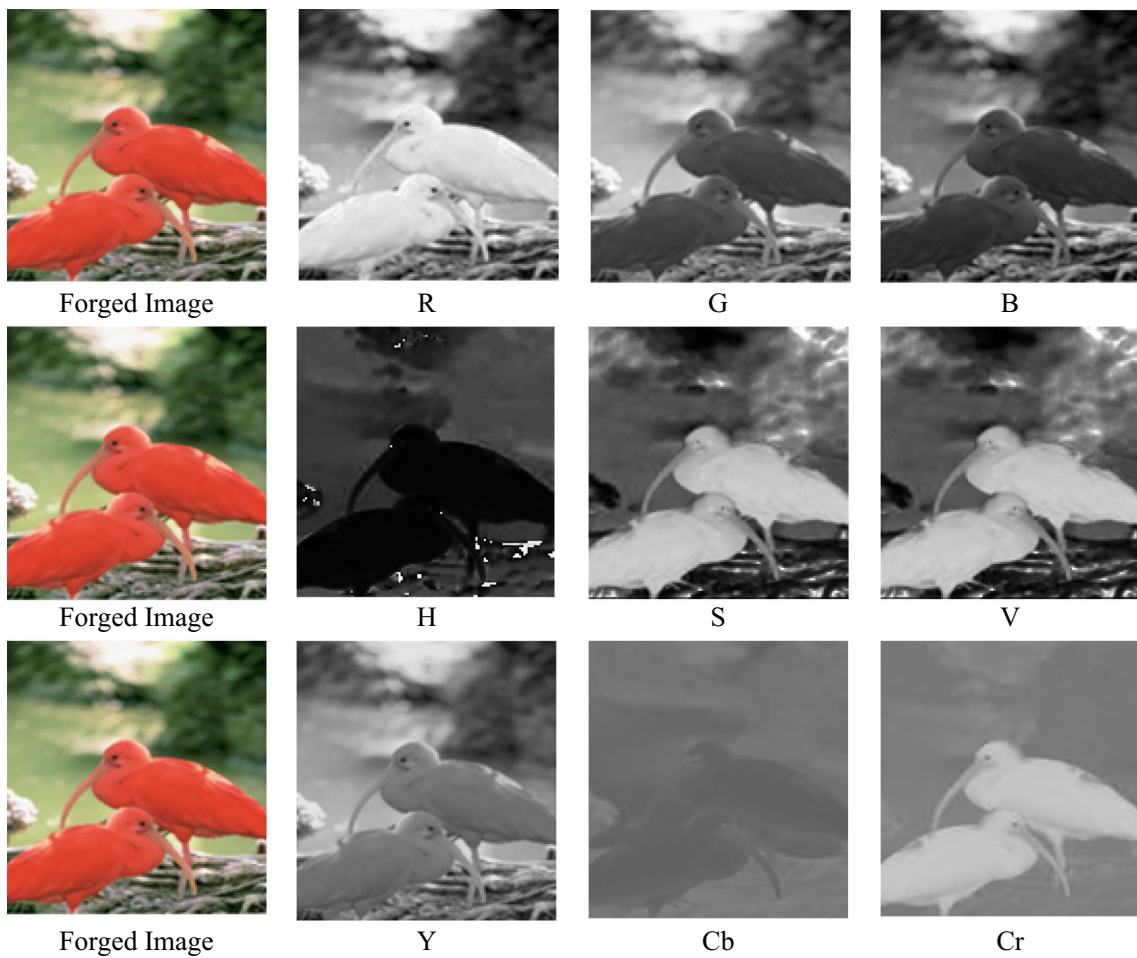


Fig. 4 Visualization of R, G, B, Y, Cb, Cr, H, S and V channels of a forged image, using RGB, YCbCr and HSV color spaces from left to right
Row1, Row2 and Row 3, respectively

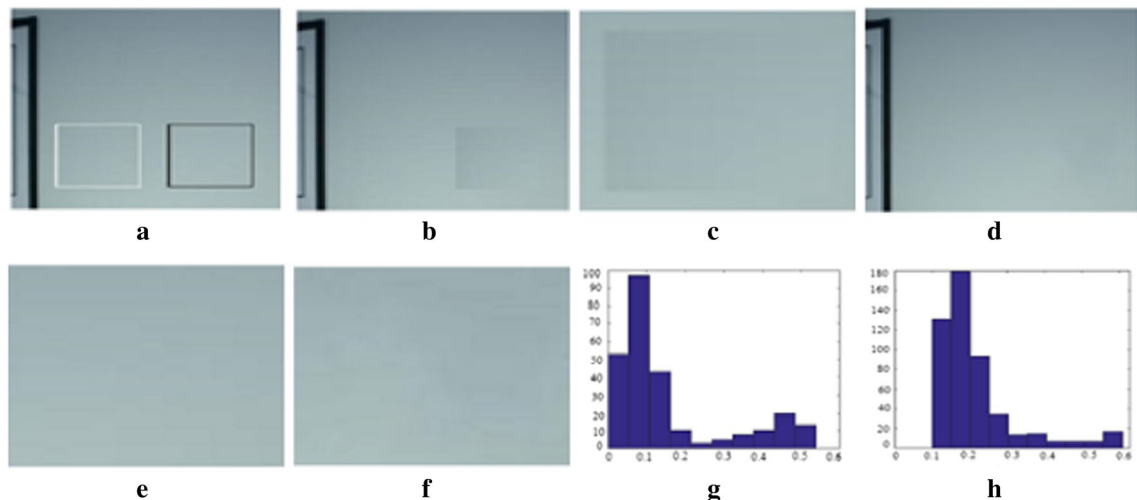


Fig. 5 **a** Region to be copied (white box), region to be forged (black box), **b** forged image, **c** zoomed-in view of forged region before post-processing, **d** post-processed forged image, **e** zoomed-in view of region (black box) before forgery, **f** zoomed-in view of forged region

(black box) after forgery and post-processing, **g** histogram of DRLBP descriptor of region (black box) before forgery (features value along x-axis and frequency along y-axis), **h** histogram of DRLBP descriptor of region (black box) after forgery

region before forgery and after forgery are almost similar (see Fig. 5e, f) because tampering artifacts are invisible to human eyes after post-processing but are still present in the forged image. DRLBP texture descriptor is employed on the chrominance components of a given image to encode these structural changes due to its capability of combining edge and texture information in a single representation. The DRLBP histograms of the authentic and tampered regions are plotted in Fig. 5g, h, respectively, and show that the features are discriminative.

3.2.1 Computation of DRLBP descriptor

An overview of computing the DRLBP descriptor is given in the following; for details, see [17, 42]. DRLBP descriptor first encodes local changes in the form of LBP codes and then estimates their distribution considering the local gradient magnitude at the corresponding locations, i.e., the DRLBP descriptor encodes the local change considering the amount of change. First, LBP codes with radius 1 and neighborhood 8 are calculated from the image, and then, the weighted histogram W_{LBP} of LBP codes is computed using the following equation:

$$W_{LBP}(i) = \sum_{x=0}^{M-1} \sum_{y=0}^{N-1} w\delta(LBP_{x,y}, i), i = 0, 1, \dots, n-1, \quad (2)$$

$$\delta(j, i) = \begin{cases} 1, & j = i \\ 0, & \text{otherwise} \end{cases}$$

where $n (=2^8)$ is the number of LBP codes, i.e., the number of bins in the histogram, w is the gradient magnitude of the pixel at location (x, y) , which weights the contribution of the corresponding LBP code according to the amount of local change at the pixel, and $M \times N$ is the resolution of the chrominance component. To remove the effect of the reversal

in the foreground and the background, a robust weighted histogram W_{RLBP} is calculated using W_{LBP} as follows:

$$W_{RLBP}(i) = W_{LBP}(i) + W_{LBP}(2^8 - 1 - i), 0 \leq i < 2^7. \quad (3)$$

Further, to enhance the discriminative effect of patterns, a discriminative weighted histogram W_{DLBP} is calculated as follows:

$$W_{DLBP}(i) = |W_{LBP}(i) - W_{LBP}(2^8 - 1 - i)|, 0 \leq i < 2^7. \quad (4)$$

The DRLBP is constructed by concatenating the robust LBP and the discriminative LBP as follows:

$$DRLBP = \{W_{RLBP}, W_{DLBP}\}. \quad (5)$$

After calculating DRLBP histogram from each channel $Ch\{Cb, Cr\}$ of the given image, the DRLBP descriptor (fv) is calculated by concatenating the DRLBP histograms corresponding to channels $Ch\{Cb, Cr\}$ as follows:

$$fv = [fv^{Cb}, fv^{Cr}]. \quad (6)$$

The descriptor fv computes the overall distribution of changes occurred due to forgery without taking into consideration their spatial locations. The incorporation of the information regarding spatial locations of patterns into fv further enhances its discriminative potential because forgery cues are of small scale and spatially localized. If features are extracted from an image, the spatial location of forgery cues may be lost. For this reason, we divide each channel of image into K blocks (sub-images), B_1, B_2, \dots, B_K each of resolution $l \times m$ such that $K(l \times m) = M \times N$. The descriptor fvB_i is computed from each block B_i , and all descriptors are concatenated to form the descriptor fv^{Ch} of each channel $Ch\{Cb, Cr\}$, i.e., $fv^{Ch} = [fv_1^{Ch}, fv_2^{Ch}, \dots, fv_K^{Ch}]$. In this way, the dimension of fv for Cb or Cr is $(RLBP_{bins} + DLBP_{bins}) \times K$. Finally, the DRLBP descriptor representing the input image is obtained using (6). The whole process of the computation of fv is detailed in Algorithm 1.

Algorithm 1: The computation of DRLBP descriptor of a given image.

Input: RGB image I , the number K of blocks

Output: DRLBP based feature vector fv

Procedure:

1. For a given image I extract chrominance components
 - a. $Ch \in \{Cb, Cr\}$
2. For each $Ch \in \{Cb, Cr\}$
 - a. Divide Ch into K blocks: B_1, B_2, \dots, B_K
 - b. For each block $B_k, k = 1, 2, \dots, K$
 - Compute DRLBP histogram fv_k^{Ch}
 - c. $fv^{Ch} = [fv_1^{Ch}, fv_2^{Ch}, \dots, fv_K^{Ch}]$
3. $fv = [fv^{Cb}, fv^{Cr}]$

Fig. 6 Histograms of pairwise distances of DRLBP features of CASIA v2.0 dataset; **a** pairwise distances within authentic class, **b** pairwise distance within forged class and **c** pairwise distance between authentic and forged classes

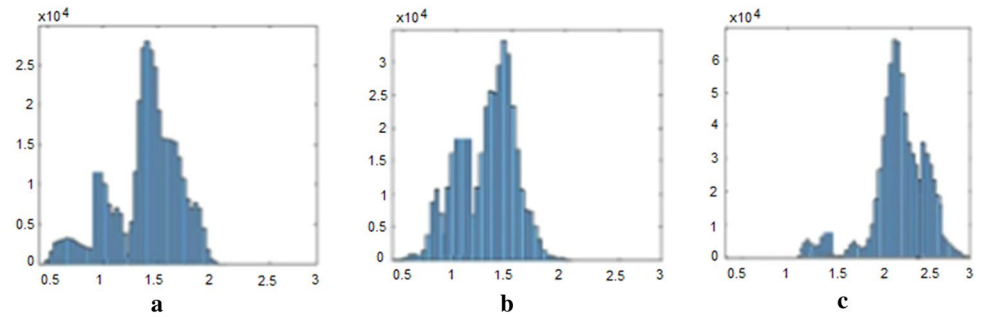


Table 1 Trace of WS and BS on DRLBP features of benchmark datasets

Dataset	Trace of WS	Trace of BS
CASIA v1.0 [45]	1.24	2.87
CASIA v2.0 [45]	1.37	2.57
CoMFoD [9]	1.48	2.21
MICC-F2000 [10]	1.28	2.01
FRITH	1.47	2.35

3.2.2 Statistical analysis of the DRLBP descriptor

To show that the DRLBP descriptor has the potential to discriminate authentic and tampered images, we give a statistical analysis of the descriptor in two different ways.

First, we computed the pairwise distances for the three cases using the city block between (i) authentic images, (ii) forged images and (iii) authentic and forged images of CASIA v2.0. The cases (i) and (ii) represent intra-class distances, whereas case (iii) represents inter-class distances; Fig. 6 shows the histograms of the three cases. Most of the pairwise distances for the intra-class cases (Fig. 6a, b) are between 0.0 and 2.00, while those for the inter-class cases (Fig. 6c) are between 1.5 and 2.5. There is an overlap of approximately 6% between pairwise distances belonging to intra-class and inter-class cases. This indicates that the DRLBP descriptor has the potential for discriminating the authentic and forged images. The effect of the overlap is reduced when a kernel SVM is used for classification

because the kernel computes the distances in a higher dimensional space where the patterns become separable.

Secondly, the effect of DRLBP descriptor is analyzed using scatter matrix-based measure because of its simplicity [43, 44]. For this purpose, two scatter matrices are used: (i) within-class scatter matrix (*WS*) and (ii) between-class scatter matrix (*BS*). *WS* and *BS* are defined as follows:

$$WS = \sum_{i=1}^c \sum_{j=1}^{N_i} (x_{ij} - \bar{x}_i)(x_{ij} - \bar{x}_i)^T, \quad (7)$$

$$BS = \sum_{i=1}^c N_i (\bar{x}_i - \bar{x})(\bar{x}_i - \bar{x})^T, \quad (8)$$

where x_{ij} is the feature space, N_i is the number of samples in i^{th} class, \bar{x}_i is the mean vector for the i^{th} class, \bar{x} is the mean vector for all classes and c is the number of classes. The traces of *WS* and *BS* represent intra-class and inter-class scatters, respectively. The features are discriminative if the intra-class scatter is small and the inter-class scatter is high. Table 1 shows the traces of *WS* and *BS* of five datasets. In each case, the trace of *BS* is high and *WS* is small, indicating that the DRLBP descriptor is discriminative (see Table 1).

3.3 Classification model training (building)

To identify an image as authentic or forged is a two-class problem. The process of training a classification SVM model is described in Algorithm 2.

Algorithm 2: Image Forgery Detection Model Training (Building) Procedure.

Input: X_t is the set of forged/tampered images, X_a , is the set of authentic images, c and g (gamma) are the parameters of SVM with RBF kernel, c_{min} , g_{min} , c_{max} and g_{max} are minimum and maximum values of c (to handle misclassification) and g (to handle non-linear classification) respectively.

Output: Trained classification model SVM

Procedure:

1. **for** each image I_i in X_t
 - Create features vector $f\nu_i$ for each tampered image using Algorithm 1
 - $tf\nu_i = f\nu_i$
 - Create labeled featured vector $tf\nu_iL$ by assigning label 1 to $tf\nu_i$**end for**
2. **for** each image I_i in X_a
 - Create features vector $f\nu_i$ for each authentic image using Algorithm 1
 - $af\nu_i = f\nu_i$
 - Create labeled featured vector $af\nu_iL$ by assigning label -1 to $af\nu_i$**end for**
3. $D \leftarrow tf\nu_iL \cup af\nu_iL$
4. $AC = 0$,
5. **for** $c = c_{min}$ to c_{max} **do**
6. **for** $g = g_{min}$ to g_{max} **do**
 - Divide D into equally k folds ($k = 10$)
 - for** $i = 1$ to k **do**
 - Train SVM(c, g) on D/F_i to get model MSVM (c, g) % all training data D except i th fold F_i
 - Test MSVM (c, g) on fold F_i
 - Record the $ACC(i)$ on fold F_i**end for**
 - $AvgACC = \frac{1}{k} \sum_{i=1}^k ACC(i)$ % compute average accuracy on k folds
 - if** $AvgACC > ACC$
 - $ACC = AvgACC, c_{opt} = c, g_{opt} = g$**end if****end for**
end for7. Fit the SVM (c_{opt}, g_{opt}) model on training data

SVM [46] deals with two-class problems by its construction and provides better generalization among kernel-based classifiers [47–49]. The SVM has a variety of kernel functions such as radial basis function (RBF), polynomial and sigmoid kernels.

Experiments are performed using these three kernels to find an optimal kernel. Experiments for identifying the optimal parameters representing the classification are performed using individual dataset or combination of datasets. A cross-validation (CV) protocol is used to divide each dataset or combination of datasets into k -fold (tenfold). The SVM parameters are tuned on the training examples (ninefold out of the tenfold), and that parameterization is used on the remaining (unused) fold. Each time the testing fold changes, the parameters are recalculated using $k-1$ -fold on k iterations. Finally, the average value of k iterations parameters is considered the final value of the trained model. All experiments are performed using the standard Lib-SVM [50], because SVM finds an optimal hyperplane

with maximum margin between the two classes [46]. SVM uses the posterior probability of classification score which is the signed distance of a sample point from the decision boundary. The positive score classifies the sample point as positive; otherwise, it is classified as negative [51].

3.4 Pre-trained model testing using cross-dataset

Further experiments are performed to ensure the generalizability of the proposed image classification approach using the cross-dataset evaluation. In this process, the features of the test image are extracted and passed to the trained model to classify whether the image is authentic or forged.

Table 2 Datasets description used for evaluation of image forgery detection algorithms and cross-dataset validation

Sr. no.	Dataset name	Authentic	Forged	Forgery types	Image resolution	Image formats	Geometric operations	Post-processing operations
1	DVM	183	180	Splicing	757×568 to 1152×768	TIFF and BMP	No	Uncompressed
2	CASIA v1.0	800	925	Splicing and copy-move	384×256	JPEG	Resize, rotation deform and distortion	Blurring, JPEG compression
3	CASIA v2.0	7491	5123	Splicing and copy-move	240×160 900×600	TIFF, JPEG and BMP	Resize, rotation and distortion	Blurring, JPEG compression
4	CoMFoD	5000	5000	Copy-move	512×512	BMP	JPEG compression, noise adding, blurring, brightness change, color reduction and contrast adjustment	
5	UNISA	2000	2000	Splicing and copy-move	4928×3264 6016×4016	TIFF, JPEG	Scaling, rotation and distortion	JPEG compression, blurring
6	FRITH	155	255	Copy-move, splicing, retouching, false captioning, fake objects insertion, image enhancement	Variety of dimensions	JPEG, TIFF, PNG, BMP	Scaling, rotation, shearing, deform and distortion	Uncompressed, JPEG compression, blurring, noise adding, brightness change color reduction and image enhancement
7	MICC-F220	111	110	Copy-move	737×492	JPEG	Scaling and rotation	JPEG compression
8	MICC-F2000	1300	700	Splicing and copy-move	2048×1536	JPEG	Scaling and rotation	JPEG compression blurring noise adding contrast adjustment
9	Set-A	13,474	13,228	Set-A is a combination of DVM, CASIA v1.0, CASIA v2.0 and CoMFoD datasets				
10	Set-B	3566	3065	Set-B is a combination of MICC-F220, MICC-F2000, UNISA and FRITH datasets				

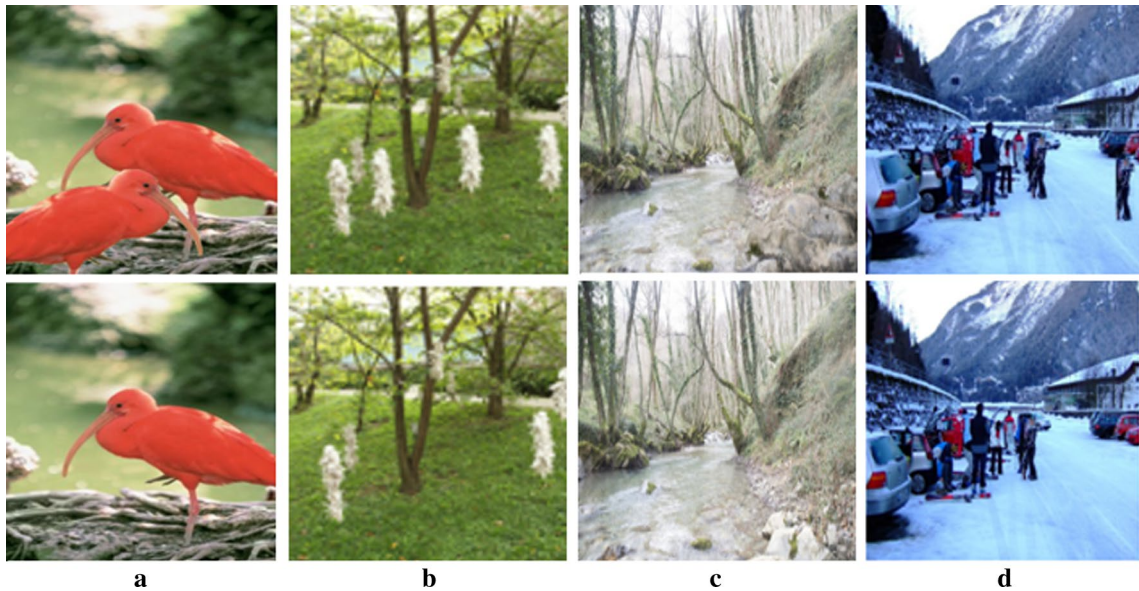


Fig. 7 Authentic (bottom), forged (top). **a** CASIA v2.0: A bird object is copied, rotated and then pasted to another location of the same image. **b** CoMFoD: The white object is multiply cloned in different locations of same image. **c** UNISA: In the forged image, the rock is

spliced at the bottom right corner of the authentic image. **d** MICC-F2000: In the forged image, an object is pasted at the right-hand side of the authentic image

4 Datasets and evaluation criteria

To build a reliable and robust image forgery detection model, training and testing on benchmark datasets are very important. We need authentic as well as forged images in datasets. Forged images should contain as many possible varieties of geometric and post-processing operations as possible. Further, for testing a trained image forgery model on unseen images, a collection of real forged images is very important to ensure the reliability of the trained model for real practical applications. In consideration of the above facts, a description of carefully selected datasets for use in our research is given in the next subsection. Furthermore, to measure the performance of any classification model, a selection of appropriate evaluation measures is necessary. This is described in Sect. 4.2.

4.1 Datasets description

Image forgery evaluation datasets are created using different cameras and image editing software packages. Publicly available benchmark datasets: Columbia color DVMM (DVMM) [52], CASIA v1.0 [45], CASIA v2.0 [45], CoMFoD [9], UNISA [35], MICC-F220 [10] and MICC-F2000 [10], are used to evaluate and validate the proposed approach. A comprehensive experimental analysis is also performed by combining different datasets with the aim that performance may improve by increasing both variety

and sample size of data. Set-A and Set-B are a combination of different datasets to analyze the impact of different formats, resolutions, geometric and post-processing operations on image forgery detection. The datasets are grouped into Set-A or Set-B based on benchmarks, forgery types, post-processing operations and number of authentic/forged images. Details of each dataset characteristics such as number of authentic and forged images, forgery types, file types, resolution, geometric and post-processing operations applied on images to make the dataset challenging are given in Table 2. An example of authentic and forged images from CASIA v2.0, CoMFoD, UNISA and MICC-F2000 is shown in Fig. 7.

4.1.1 Forged real images throughout history (FRITH), a new dataset for evaluation of image forgery detection

In the forensic literature, many publicly available benchmarks datasets have been used for the detection of specific types of image forgeries. These benchmark datasets have been developed for supporting copy–move and splicing forgeries, having specific file formats, resolutions, geometric and post-processing operations. For example, the DVMM dataset has uncompressed authentic and forged images of sizes 757×568 and 1152×768 pixels. The CASIA v1.0 dataset has authentic and spliced images of size 384×256 pixels. The CoMFoD dataset has 200 sets of images of size 512×512 , each set containing authentic and forged



Fig. 8 Examples of authentic (bottom) and forged (top) images from the FRITH dataset: **a** A doctored image showing Jeffrey Wong receiving an award, **b** tampered image of Obama's meeting with Iranian President Hassan Rouhani, **c** the Boston Marathon bombing tampered

photo showing less disturbing content, **d** a digitally altered puddle of water made to appear as blood flowing from the temple of Hatshepsut in Luxor Egypt

examples. Both authentic and forged images were post-processed to enlarge the size of dataset (10,400 post-processed authentic and forged images). MICC-F220 consists of 220 images, while MICC-F2000 contains 2000 images, all 2048×1536 pixels. The existing benchmark datasets have been created artificially by academic researchers with a specific goal in mind, primarily for the purposes of testing their algorithms only. However, in most cases the forgeries are fairly crude and made by experts with the intention of forgery detection. We validated that the purpose of applying post-processing operations is to create semantically meaningful forged images. To the best of our knowledge, the applicability of existing benchmark datasets to realistic scenarios is always limited. Therefore, a benchmark dataset of semantically meaningful forged images used intentionally for false propaganda or malpractices should be made available to the researchers for the reliable testing of image forgery detection algorithms. Therefore, a new benchmark dataset has been created and labeled as Forged Real Images Throughout History (FRITH), consisting of real forgeries including many famous examples [53].

The collection of forgeries in [53] provided the starting point of creating FRITH. However, mostly [53] just contains a single image for each type of forgery and generally does not provide the source of authentic images. For proper evaluation of image forgery detection, we require a dataset consisting of both authentic and forged image sets. Therefore, we used the forged images from [53] as queries in an internet search and selected the best quality versions of the matches to provide both the forged and their authentic samples. In total, 255 historic forged images were collected. Among these, authentic (untampered) versions of 155 forged images are also obtained.

The dataset has many challenging characteristics such as (i) many images have been scanned as the originals were not digital and (ii) the forged images contain a variety of image forgeries such as copy-move and splicing forgeries by transferring objects or regions, forgery by inserting fake objects, manipulation of existing objects, forged images being post-processed using lightening effects and image enhancement/tuning operations. The FRITH dataset has enough variety of real copy-move and splicing forgeries, in addition to other types of forgeries such as fake objects insertion, false captioning and image enhancement operations. In future versions, we plan to add more real forged images with their authentic ones. The dataset¹ is available for the public usage. Example images of FRITH are shown in Fig. 8, and its detail is listed in Table 2.

4.2 Evaluation criteria

Accuracy (*ACC*), true positive rate (*TPR*), true negative rate (*TNR*), *F-Measure* and area under ROC curve (*AUC*) are widely used to evaluate image forgery detection techniques [54, 55]. We evaluate our proposed approach using *ACC*, *TPR*, *TNR*, *F-Measure* and *AUC* with cross-dataset evaluation. The evaluation measures are defined as follows.

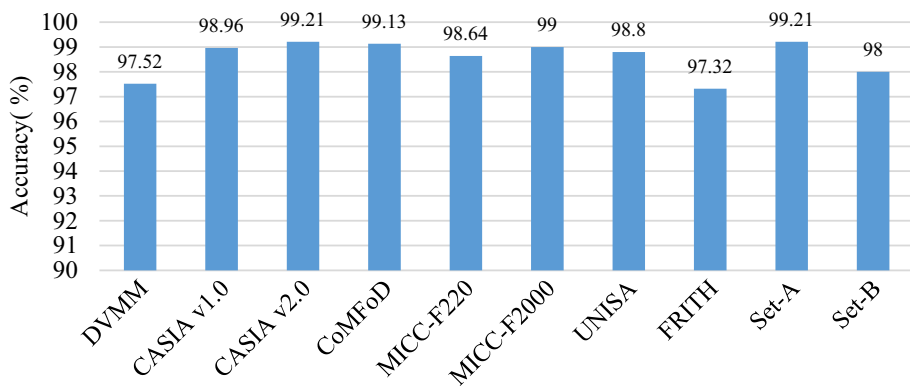
Accuracy (*ACC*)

Accuracy is the proportion of correctly predicted authentic and forged images and is defined as:

$$ACC = \frac{(TP + TN)}{TP + TN + FN + FP} \times 100\%, \quad (9)$$

¹ The FRITH dataset can be downloaded from <http://users.cs.cf.ac.uk/Paul.Rosin/#data>

Fig. 9 Classification accuracy of proposed method on different datasets in terms of training on same dataset and testing on same dataset



where true positive (TP) is the number of tampered images, which are classified as tampered; false negative (FN) is the number of tampered images, which are classified as authentic; true negative (TN) is the number of authentic images, which are classified as authentic; and false positive (FP) is the number of authentic images, which are classified as tampered ones.

True positive rate (TPR)

TPR also known as sensitivity (SN) is the probability of recognizing a tampered image as tampered and is computed as follows:

$$TPR = SN = \frac{TP}{TP + FN} \times 100\%. \quad (10)$$

True negative rate (TNR)

TNR also known as specificity (SP) is the probability of recognizing an authentic image as authentic and is computed as follows:

$$TNR = SP = \frac{TN}{TN + FP} \times 100\%. \quad (11)$$

F-Measure

F-Measure is the harmonic mean of precision and sensitivity and is computed as follows:

$$F - Measure = \frac{2TP}{2TP + FP + FN}. \quad (12)$$

Area under the curve (AUC) of receiver operating characteristic (ROC)

The ROC curve is used to present the performance of the binary classifier. It plots TPR versus FPR for exclusive thresholds of the classifier significances [56].

Cross-dataset evaluation

Cross-dataset evaluation (training on one dataset and testing on another dataset) is the ultimate evaluation to expose the weaknesses and ensure the robustness of any image forgery detection method. In our experimental analysis, the performance of image forgery detection is evaluated using cross-dataset protocol.

5 System parameters

To find the best parameters of the system, we performed a series of experiments by considering different combinations. C_b and C_r components are found suitable due to their better performance during experiments as also referred in methods [1, 29, 31, 41]. For calculating the DRLBP features, each component is divided into overlapped blocks with 20% overlapping rate. In the case of DRLBP, we found that the uniform (u_2) LBP (maximum two-bit transitions) with $P=8$ and $R=1$ is an appropriate choice due to its better performance as referred in [17].

The optimization of the SVM parameters was done using the training datasets, and we found that the RBF kernel had the best performance. The RBF kernel involves two parameters: c and g . The setting of these parameters plays a significant role in classification. The parameter c is used to balance the model complexity by fitting minimum error rate. The kernel function parameter g is used to determine the nonlinear mapping from the input space to the high-dimensional feature space [57]. Kernel parameters, c and g , were tuned using a grid-search method and found $c = 2^5$ and $g = 2^{-5}$ best. Different k-fold cross-validations (CV) such as fivefold, sevenfold and tenfold were considered to best fit training data on classification model, and we found that tenfold CV was most appropriate due to its lower sensitivity while dividing data for training and testing/validation for model fitting.

6 Experimental results, comparison and discussion

The classification accuracy of the proposed method on different datasets is presented in Fig. 9.

The results reported here were obtained using the optimal parameters values of the system.

Table 3 Comparison of proposed method with recent state-of-the-art methods in terms of training and testing on same dataset

Training and testing datasets	Approaches	ACC (%)	TPR (%)	TNR (%)	F-Measure	AUC
DVMM	Proposed	97.52	96.67	98.36	0.97	0.97
	Alahmadi et al. [58]	96.66	96.33	79.09	–	0.96
	Hussain et al. [34]	94.19	–	–	–	–
	Muhammad et al. [31]	96.39	–	–	–	–
	Rao and Ni [59]	96.38	–	–	–	–
	Pham et al. [37]	96.90	–	–	–	–
	Wang and Kamata [38]	82.31	–	–	–	–
	Proposed	98.96	99.03	98.88	0.99	0.98
	Alahmadi et al. [58]	97.00	98.24	97.07	–	0.97
	Shen et al. [60]	97.00	–	–	–	–
CASIA v1.0	El-Alfy and Qureshi [1]	98.65	98.80	98.39	–	0.99
	Goh and Thing [61]	90.18	–	–	–	–
	Hussain et al. [34]	96.53	–	–	–	–
	Muhammad et al. [31]	94.89	93.91	–	–	0.93
	Rao and Ni [59]	98.04	–	–	–	–
	Pham et al. [37]	96.90	–	–	–	–
	Proposed	99.21	99.02	99.33	0.99	0.99
	Cattaneo et al. [35]	90.00	–	–	–	–
	Alahmadi et al. [58]	97.50	98.45	96.84	–	0.97
	Rota et al. [33]	97.44	96.16	97.44	–	0.99
CASIA v2.0	Shen et al. [60]	98.00	–	–	–	–
	El-Alfy and Qureshi [1]	99.00	99.55	99.65	–	0.99
	Hussain et al. [34]	94.17	–	–	–	–
	Muhammad et al. [31]	97.33	98.50	–	–	0.97
	Rao and Ni [59]	97.83	–	–	–	–
	Pham et al. [37]	96.90	–	–	–	–
	Proposed	99.64	99.9	99.20	0.99	0.99
	Amerini et al. [10]	–	98.21	91.84	–	–
	Wang and Kamata [38]	98.92	–	–	–	–
	Proposed	99.64	98.57	99.23	0.99	0.99
MICC-F220	Amerini et al. [10]	–	93.43	89.04	–	–
	Wang and Kamata [38]	99.14	–	–	–	–
	Proposed	99.10	99.20	99.18	0.99	0.99
	Cattaneo et al. [35]	92.88	93.74	92.03	0.93	0.92
	Hussain et al. [34]	97.37	98.28	96.48	0.97	0.97
	Alahmadi et al. [58]	97.50	98.45	96.84	0.97	0.97
	Wang et al. [38]	98.00	98.00	98.00	0.98	0.98
	Proposed	98.02	97.88	98.15	0.98	0.98
	Cattaneo et al. [35]	89.88	88.09	91.42	0.89	0.90
	Hussain et al. [34]	96.52	96.25	96.75	0.96	0.96
Set-A	Alahmadi et al. [58]	97.50	98.45	96.84	0.97	0.97
	Wang et al. [38]	97.41	96.00	96.57	0.97	0.97
	Proposed	99.10	99.20	99.18	0.99	0.99
	Cattaneo et al. [35]	92.88	93.74	92.03	0.93	0.92
	Hussain et al. [34]	97.37	98.28	96.48	0.97	0.97
Set-B	Alahmadi et al. [58]	97.50	98.45	96.84	0.97	0.97
	Wang et al. [38]	98.00	98.00	98.00	0.98	0.98
	Proposed	98.02	97.88	98.15	0.98	0.98
	Cattaneo et al. [35]	89.88	88.09	91.42	0.89	0.90
	Hussain et al. [34]	96.52	96.25	96.75	0.96	0.96

6.1 Comparison of proposed method terms of training and testing on the same dataset

In this section, the results of the proposed method and state-of-the-art methods are compared, in terms of training and testing on same dataset (see Table 3).

The comparison shows that the proposed method has better performance on different datasets in terms of training and testing on the same dataset, and the proposed method is robust against different geometric and post-processing operations applied on forged images of these datasets. The reason for this robustness is the ability of the DRLBP texture

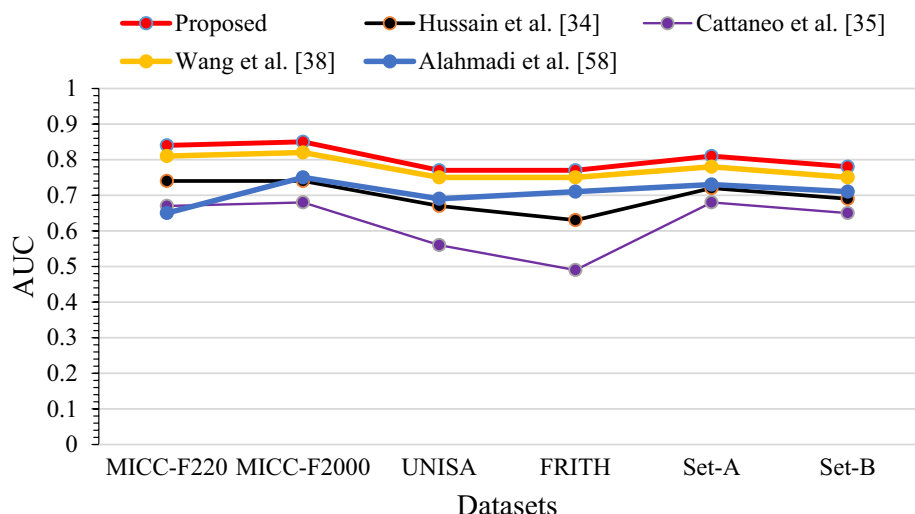
Table 4 Comparison of the proposed method and other recent state-of-the-art methods on cross-dataset evaluation. Testing dataset results are reported

Testing dataset	Training dataset	Approaches	ACC (%)	TPR (%)	TNR (%)	F-Measure	AUC
MICC-F220	Set-A	Proposed	84.16	86.36	81.98	0.84	0.84
		Cattaneo et al. [35]	67.12	61.26	72.97	0.65	0.67
		Hussain et al. [34]	74.21	70.91	77.48	0.73	0.74
		Alahmadi et al. [58]	65.33	60.34	71.97	0.64	0.65
		Wang et al. [38]	82.61	83.63	80.89	0.81	0.81
MICC-F2000	Set-A	Proposed	86.50	83.33	88.46	0.81	0.85
		Cattaneo et al. [35]	69.75	56.43	76.92	0.67	0.68
		Hussain et al. [34]	76.11	70.71	78.95	0.73	0.74
		Alahmadi et al. [58]	75.00	74.17	77.59	0.75	0.75
		Wang et al. [38]	83.05	84.13	84.16	0.82	0.82
UNISA	Set-A	Proposed	77.46	85.00	70.00	0.79	0.77
		Cattaneo et al. [35]	56.25	60.00	52.50	0.58	0.56
		Hussain et al. [34]	67.50	70.00	65.00	0.68	0.67
		Alahmadi et al. [58]	68.05	72.00	67.90	0.69	0.69
		Wang et al. [38]	75.34	80.20	68.29	0.75	0.75
FRITH	Set-A	Proposed	74.39	72.55	77.42	0.78	0.77
		Cattaneo et al. [35]	48.78	47.60	51.61	0.53	0.49
		Hussain et al. [34]	63.41	62.75	64.25	0.66	0.63
		Alahmadi et al. [58]	69.94	68.57	69.52	0.71	0.71
		Wang et al. [38]	72.93	71.15	75.24	0.75	0.75

Table 5 Comparison of the proposed method and other state-of-the-art methods on cross-dataset evaluation. Testing dataset results are reported

Testing dataset	Training dataset	Approaches	ACC (%)	TPR (%)	TNR (%)	F-Measure	AUC
Set-A	Set-B	Proposed	81.27	81.10	81.45	0.81	0.81
		Cattaneo et al. [35]	68.54	68.25	68.83	0.68	0.68
		Hussain et al. [34]	72.29	72.03	72.54	0.72	0.72
		Alahmadi et al. [58]	73.92	73.30	73.45	0.73	0.73
		Wang et al. [38]	79.72	78.01	78.39	0.78	0.78
Set-B	Set-A	Proposed	77.89	77.16	78.52	0.76	0.78
		Cattaneo et al. [35]	66.10	60.85	70.89	0.63	0.65
		Hussain et al. [34]	69.84	67.37	71.96	0.67	0.69
		Alahmadi et al. [58]	70.29	71.13	72.54	0.71	0.71
		Wang et al. [38]	76.98	75.61	77.25	0.75	0.75

Fig. 10 AUC comparison of the proposed method, Hussain et al. and Cattaneo et al., testing dataset/training dataset (MICC-F220/Set-A, MICC-F2000/Set-A, UNISA/Set-A, FRITH/Set-A, Set-A/Set-B and Set-B/Set-A)



descriptor to model the structural changes in images that occurred due to forgery. The results of the proposed method are also comparable with the method of Yan et al. [40] which is trained using CNN architecture. The proposed method best detection accuracy on the combination of different datasets is 99.10%, while the Yan et al. method best detection accuracy is 86.89%.

6.2 Comparison of proposed method in terms of training and testing on different datasets

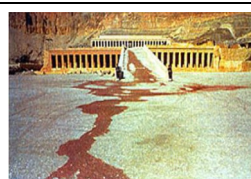
Usually, the same dataset is divided into two parts for training and testing or an n-fold strategy is applied but on the same dataset. For successful practical applications, it is necessary to develop the model through the process of training/validating on one dataset and finally testing on another dataset acquired from different sources, which is called cross-dataset validation. For this purpose, four state-of-the-art methods [34, 35, 38, 58] are implemented together with the proposed approach.

A series of experiments were performed to analyze the performance of the proposed method on cross-dataset testing. We trained the model on Set-A dataset and then tested it on the MICC-F220, MICC-F2000, UNISA and FRITH datasets (see Table 4).

To determine the robustness of the image forgery classification model, experiments were performed by training the model on the Set-A dataset and then testing it on the Set-B dataset and vice versa (see Table 5). The cross-dataset performance of the proposed system is better than the state-of-the-art methods, which indicates that the proposed method has better robustness.

Our work adds to previous reports using cross-dataset testing, which is an important area of research and an important component in real practice where different images need to be classified. Our experiments with cross-dataset testing showed that our proposed method achieved better performance than those of [34, 35, 38, 58] (see Fig. 10).

Table 6 Example images of failure cases of forged images from the FRITH dataset

	<p>In this image text in the passport is manipulated and the image of the passport is used to gain some illegal benefit. The person in the image altered his particulars to hide the passport contents</p>
	<p>The Polish subsidiary of Microsoft ran a version of a company marketing campaign in which the photo was altered by replacing the face of middle person</p>
	<p>The image was August 2007 cover of the scientific publication Nature showing three aircrafts measuring atmospheric pressure. The top and bottom aircrafts are cloned</p>
	<p>In this image the Swiss tabloid Blick digitally altered a puddle of water to appear as blood flowing from the temple to show a terrorist attack at the temple of Hatshepsut in Luxor Egypt</p>
	<p>In the image Al Franken is shown dressed up like a baby bunny, wearing adult diapers and clutching a fluffy white teddy bear is fake</p>

6.3 Discussion

The objective of this paper was to perform a comprehensive analysis of image forgery detection algorithms and the role of datasets used to evaluate these algorithms. We introduced an edge–texture feature-based approach for classifying authentic and tampered images. The novelty in our experimental analysis is that: (i) we explored state-of-the-art texture descriptors and found DRLBP to be a robust texture descriptor, which models the structural changes occurred in images due to forgery using edge–texture features that incorporate information such as texture, boundary discontinuities and inconsistencies; (ii) we validated our approach and four state-of-the-art methods [34, 35, 38, 58] by performing a series of experiments on publicly available datasets; and (iii) we also prepared a new dataset FRITH to evaluate an image forgery detection technique on forged images used intentionally for false propaganda or malpractices rather than datasets designed specifically by academic researchers. From the experimental analysis, it is observed that success of any forgery detection system depends on: (i) modeling the artifacts of forgery in a precise way; (ii) training a model on samples with as many as possible different types of forgeries, geometric transformations and post-processing operations rather than increasing the size of samples in general.

Detecting forgery that has been carried out by inserting a new object or manipulating an existing object is also a challenging task. Scene lighting and geometry parameters may help to detect such tampering. Experiments revealed that exploiting the texture of such suspected images may give a reasonable cue to detect such tampering. We recommend that there must be a large dataset containing object insertion and manipulation forgeries, such as FRITH (it has some examples of such manipulations), to ensure the robustness of an image forgery detection system in real scenarios.

Erasing manipulations disturb the structural changes occurred in images due to forgery and can be traced by exploiting the JPEG compression artifacts, if the original images were compressed after such tampering. From a forensics point of view, forgery by means of changing the lighting conditions of an image is dangerous due to their potential of concealing forgeries. For example, a splicing forgery may be concealed by changing the lightening parameters. Again, JPEG compression artifacts may help to find such traces.

Image enhancement operations, such as blurring (filtering), noise and contrast adjustment, are applied on forged images with the intention to remove low-level traces of forgery. We observed from the experimental analysis by counting small pixel fluctuations and having texture information together with edges that it is possible to detect such traces because image enhancement operations only soften the edges, and not erase them completely.

6.3.1 Failure analysis

The proposed method achieved good performance and, however, is less effective for some cases. The proposed method and methods in [34, 35, 38, 58] failed to predict some real forgeries given in Table 6. After analyzing the failure cases, it is found that texture and edges of the forged images contain a mix of colors from the foreground and background of the source image which is still a challenge. We will address such problems in the future by exploring manipulation-relevant features using deep learning approaches.

7 Conclusion and future work

In this paper, a novel image forgery detection method based on DRLBP and SVM has been proposed. The chrominance components of an input image are divided into overlapping blocks, and then, the DRLBP code of each block is calculated. Later, histograms of all the blocks of both Cb and Cr components are used as features. Classification is performed using an SVM. The method was extensively evaluated on individual and combined benchmark datasets in terms of training and testing on splits of the same dataset and on different datasets (i.e., cross-dataset validation). The proposed method was evaluated using eight benchmark datasets and their combinations. The classification accuracy of our method is consistent across the eight datasets, and it has better performance than state-of-the-art methods due to the effective modeling structural changes occurring in tampered images by DRLBP texture descriptor. The results on combinations (Set-A and Set-B) of datasets indicate that the proposed method is robust and consistent under different post-processing operations, file types and image resolutions (small, medium and high). The cross-dataset evaluation (training on one dataset and testing on another dataset) shows that the performance of the proposed method is significantly better than state-of-the-art methods. DRLBP is an elegant texture descriptor to represent important features of image tampering and helps in classifying whether an image is tampered or authentic. Furthermore, the approach is robust against different geometric transformations and post-processing operations. Cross-dataset evaluation is the ultimate test to expose the weaknesses and robustness of any image forgery detection method.

The results of this study are better than other state-of-the-art image forgery detection methods in terms of cross-dataset validation; there is still a room for improving the approach to ensure the robustness of an image forgery detection method on unseen images. It is believed that the research community should adopt the cross-dataset validation procedure from now on. From the experimental analysis, it is considered that statistical artifacts of possible types

of image forgeries must be presented by benchmark datasets to enable the development off a robust model. As future work, it is planned to localize the tampered regions and tune the parameters using meta-heuristics methods to improve the cross-dataset validation performance. Dynamic learning of the classification method when tested on unseen images is another plan for future research.

Acknowledgement This research is supported by Higher Education Commission (HEC) Pakistan under International Research Support Initiative Program (IRSIP), grant # 1-8/HEC/HRD/2017/6950, and under Pakistan Program for Collaborative Research (PPCR), grant # 20-8/HEC/R&D/PPCR/2017, for the visit at School of Computer Science and Informatics, Cardiff University, UK, and PDE-GIR project which has received funding from the European Unions Horizon 2020 research and innovation programme under the Marie Skłodowska-Curie grant agreement No 778035, for the visit at Bournemouth University, UK.

References

- El-Alfy, E.-S.M., Qureshi, M.A.: Robust content authentication of gray and color images using lbp-dct markov-based features. *Multimed. Tools Appl.* **76**(12), 1–22 (2016)
- Khurshid, A., Zulfiqar, H., Muhammad, H.: Copy-move and splicing image forgery detection and localization techniques: a review. *Aust. J. Forensic Sci.* **49**(3), 281–307 (2017)
- Soni, B., Das, P.K., Thounaojam, D.M.: CMFD: a detailed review of block based and key feature based techniques in image copy-move forgery detection. *IET Image Process.* **12**(2), 262–282 (2017)
- Gryka, M., Terry, M., Brostow, G.J.: Learning to remove soft shadows. *ACM Trans. Gr. (TOG)* **34**(5), 153–167 (2015)
- Karsch, K., Sunkavalli, K., Hadap, S., Carr, N., Jin, H., Fonte, R., Sittig, M., Forsyth, D.: Automatic scene inference for 3D object compositing. *ACM Trans. Gr. (TOG)* **33**(3), 32 (2014)
- Gastal, E.S., Oliveira, M.M.: High-order recursive filtering of non-uniformly sampled signals for image and video processing. *Eurographics* **34**(2), 81–93 (2015)
- Liao, J., Lima, R.S., Nehab, D., Hoppe, H., Sander, P.V., Yu, J.: Automating image morphing using structural similarity on a half-way domain. *ACM Trans. Gr. (TOG)* **33**(5), 168 (2014)
- Xue, S., Agarwala, A., Dorsey, J., Rushmeier, H.: Understanding and improving the realism of image composites. *ACM Trans. Gr. (TOG)* **31**(4), 84(1)–84(10) (2012)
- Tralic, D., Zupancic, I., Grgic, S., Grgic, M.: CoMoFoD—new database for copy-move forgery detection. In: Proceedings of 55th ELMAR International Symposium, Zadar, Croatia, pp. 49–54 (2013)
- Amerini, I., Ballan, L., Caldelli, R., Del Bimbo, A., Serra, G.: A sift-based forensic method for copy-move attack detection and transformation recovery. *IEEE Trans. Inf. Forensics Secur.* **6**(3), 1099–1110 (2011)
- Schetterer, V., Juliani, M., Piva, A., Oliveira, M.M.: Digital Image Forensics vs. Image Composition: An Indirect Arms Race. *arXiv :1601.03239* (2016)
- Birajdar, G.K., Mankar, V.H.: Digital image forgery detection using passive techniques: a survey. *Digit. Investig.* **10**(3), 226–245 (2013)
- Kamenicky, J., Bartos, M., Flusser, J., Mahdian, B., Kotera, J., Novozamsky, A., Saic, S., Sroubek, F., Sorel, M., Zita, A.: PIZ-ZARO: Forensic analysis and restoration of image and video data. *Forensic Sci. Int.* **264**, 153–166 (2016)
- Pandey, R., Singh, S., Shukla, K.: Passive forensics in image and video using noise features: a review. *Digit. Investig.* **19**(1), 1–28 (2016)
- Redi, J.A., Taktak, W., Dugelay, J.-L.: Digital image forensics: a booklet for beginners. *Multimed. Tools Appl.* **51**(1), 133–162 (2011)
- Qazi, T., Hayat, K., Khan, S.U., Madani, S.A., Khan, I.A., Kolodziej, J., Li, H., Lin, W., Yow, K.C., Xu, C.Z.: Survey on blind image forgery detection. *IET Image Process.* **7**(7), 660–670 (2013)
- Satpathy, A., Jiang, X., Eng, H.L.: LBP-based edge-texture features for object recognition. *IEEE Trans. Image Process.* **23**(5), 1953–1964 (2014)
- Chamlawi, R., Khan, A., Usman, I.: Authentication and recovery of images using multiple watermarks. *Comput. Electr. Eng.* **36**(3), 578–584 (2010)
- Lee, T.-Y., Lin, S.D.: Dual watermark for image tamper detection and recovery. *Pattern Recogn.* **41**(11), 3497–3506 (2008)
- Prathap, I., Natarajan, V., Anitha, R.: Hybrid robust watermarking for color images. *Comput. Electr. Eng.* **40**(3), 920–930 (2014)
- Al-Qershi, O.M., Khoo, B.E.: Passive detection of copy-move forgery in digital images: state-of-the-art. *Forensic Sci. Int.* **231**(1), 284–295 (2013)
- Korus, P.: Digital image integrity—a survey of protection and verification techniques. *Digit. Signal Process.* **71**(5), 1–26 (2017)
- Hussain, M., Wahab, A.W.A., Idris, Y.I.B., Ho, A.T., Jung, K.-H.: Image steganography in spatial domain: a survey. *Signal Process. Image Commun.* **65**, 46–66 (2018)
- Farid, H.: Detecting Digital Forgeries Using Bispectral Analysis, Technical Report AIM-1657, AI Lab, Massachusetts Institute of Technology, Cambridge, USA (1999)
- Ng, T., Chang, S.: A model for image splicing. In: Proceedings of International Conference on Image Processing Singapore, pp. 1169–1172 (2004)
- Ng, T.T., Chang, S.F., Sun, Q.: Blind detection of photomontage using higher order statistics. In: Proceedings of International Symposium on Circuits and Systems, Vancouver, Canada, pp. 688–691 (2004)
- Ng, T.T., Chang, S.F., Sun, Q.: A data set of authentic and spliced image blocks. Columbia University, ADVENT Tech. Rep., pp. 203–204 (2004)
- Wang, W., Dong, J., Tan, T.: Effective image splicing detection based on image chroma. In: Proceedings of 16th IEEE International Conference on Image Processing, Cairo, Egypt, pp. 1257–1260 (2009)
- Wang, W., Dong, J., Tan, T.: Image tampering detection based on stationary distribution of Markov Chain. In: Proceedings of 17th IEEE International Conference on Image Processing Hong Kong, pp. 2101–2104 (2010)
- Zhao, X., Li, J., Li, S., Wang, S.: Detecting digital image splicing in chroma spaces. In: Proceedings of International Workshop on Digital Watermarking, Berlin, Germany, pp. 12–22 (2010)
- Muhammad, G., Al-Hammadi, M., Hussain, M., Bebis, G.: Image forgery detection using steerable pyramid transform and local binary pattern. *Mach. Vis. Appl.* **25**(4), 985–995 (2014)
- Cozzolino, D., Poggi, G., Verdoliva, L.: Efficient dense-field copy-move forgery detection. *IEEE Trans. Inf. Forensics Secur.* **10**(11), 2284–2297 (2015)
- Rota, P., Sangineto, E., Conotter, V., Pramerdorfer, C.: Bad teacher or unruly student: can deep learning say something in image forensics analysis? In: Proceedings of 23rd International Conference on Pattern Recognition, Cancún, Mexico, pp. 2503–2508 (2016)
- Hussain, M., Qasem, S., Bebis, G., Muhammad, G., Aboalsamh, H., Mathkour, H.: Evaluation of image forgery detection using multi-scale Weber local descriptors. *Int. J. Artif. Intell. Tools* **24**(4), 1–28 (2015)

35. Cattaneo, G., Roscigno, G., Petrillo, U.F.: Improving the experimental analysis of tampered image detection algorithms for biometric systems. *Pattern Recogn. Lett.* **113**(1), 93–101 (2017)
36. Lin, Z., He, J., Tang, X., Tang, C.-K.: Fast, automatic and fine-grained tampered JPEG image detection via DCT coefficient analysis. *Pattern Recogn.* **42**(11), 2492–2501 (2009)
37. Pham, N.T., Lee, J.-W., Kwon, G.-R., Park, C.-S.: Efficient image splicing detection algorithm based on markov features. *Multimed. Tools Appl.* **78**(9), 12405–12419 (2019)
38. Wang, L., Kamata, S.-i.: Forgery image detection via mask filter banks based CNN. In: Proceedings of 10th International Conference on Graphics and Image Processing, Chengdu, China, pp. 1–6 (2019)
39. He, K., Zhang, X., Ren, S., Sun, J.: Deep residual learning for image recognition. In: Proceedings of IEEE Conference on Computer Vision and Pattern Recognition, Las Vegas, Nevada, USA, pp. 770–778 (2016)
40. Yan, Y., Ren, W., Cao, X.: Recolored image detection via a deep discriminative model. *IEEE Trans. Inf. Forensics Secur.* **14**(1), 5–17 (2019)
41. Zhao, X., Li, S., Wang, S., Li, J., Yang, K.: Optimal chroma-like channel design for passive color image splicing detection. *EURASIP J. Adv. Signal Process.* **2012**(1), 1–11 (2012)
42. Dalal, N., Triggs, B.: Histograms of oriented gradients for human detection. In: Proceedings of IEEE Conference on Computer Vision and Pattern Recognition, San Diego, CA, USA, pp. 886–893 (2005)
43. Fukunaga, K.: Introduction to Statistical Pattern Recognition. Elsevier, Amsterdam (2013)
44. Webb, A.R.: Statistical Pattern Recognition. Wiley, Hoboken (2003)
45. Dong, J., Wang, W., Tan, T.: CASIA image tampering detection evaluation database. In: Proceedings of IEEE China Summit and International Conference on Signal and Information Processing Xi'an, China, pp. 422–426 (2013)
46. Cortes, C., Vapnik, V.: Support-vector networks. *Mach. Learn.* **20**(3), 273–297 (1995)
47. Vapnik, V.: The Nature of Statistical Learning Theory. Springer, Berlin (2013)
48. Cristianini, N., Shawe Taylor, J.: An Introduction to Support Vector Machines and Other Kernel-Based Learning Methods. Cambridge University Press, Cambridge (2000)
49. Hsu, C.W., Lin, C.J.: A comparison of methods for multiclass support vector machines. *IEEE Trans. Neural Netw.* **13**(2), 415–425 (2002)
50. Chang, C.C., Lin, C.J.: LIBSVM: a library for support vector machines. *ACM Trans. Intell. Syst. Technol. (TIST)* **2**(3), 27:1–27:10 (2011)
51. Platt, J.: Probabilistic outputs for support vector machines and comparisons to regularized likelihood methods. *Adv. Large Margin Classif.* **10**(3), 61–74 (1999)
52. Hsu, Y.-F., Chang, S.-F.: Detecting image splicing using geometry invariants and camera characteristics consistency. In: Proceedings of IEEE International Conference on Multimedia and Expo. Toronto, Canada, pp. 549–552 (2006)
53. Farid, H.: Photo tampering throughout history (2011). <http://www.cs.dartmouth.edu/farid/research/digitaltampering>. Accessed 23 June 2017
54. Richao, C., Gaobo, Y., Ningbo, Z.: Detection of object-based manipulation by the statistical features of object contour. *Forensic Sci. Int.* **236**, 164–169 (2014)
55. Su, L., Huang, T., Yang, J.: A video forgery detection algorithm based on compressive sensing. *Multimed. Tools Appl.* **74**(17), 1–16 (2014)
56. Sokolova, M., Japkowicz, N., Szpakowicz, S.: Beyond accuracy, F-score and ROC: a family of discriminant measures for performance evaluation. In: Proceedings of Australasian Joint Conference on Artificial Intelligence, Berlin, Germany, pp. 1015–1021 (2006)
57. Hussain, M., Wajid, S.K., Elzaat, A., Berbar, M.: A comparison of SVM kernel functions for breast cancer detection. In: Proceedings of International Conference on Computer Graphics, Imaging and Visualization (CGIV), Singapore, Singapore, pp. 145–150 (2011)
58. Alahmadi, A., Hussain, M., Aboalsamh, H., Muhammad, G., Bebis, G., Mathkour, H.: Passive detection of image forgery using DCT and local binary pattern. *SIViP* **11**(1), 81–88 (2017)
59. Rao, Y., Ni, J.: A deep learning approach to detection of splicing and copy-move forgeries in images. In: Proceedings of IEEE International Workshop on Information Forensics and Security (WIFS), pp. 1–6 (2016)
60. Shen, X., Shi, Z., Chen, H.: Splicing image forgery detection using textural features based on the grey level co-occurrence matrices. *IET Image Process.* **11**(1), 44–53 (2016)
61. Goh, J., Thing, V.L.: A hybrid evolutionary algorithm for feature and ensemble selection in image tampering detection. *Int. J. Electron. Secur. Digit. Forensics* **7**(1), 76–104 (2015)

Publisher's Note Springer Nature remains neutral with regard to jurisdictional claims in published maps and institutional affiliations.



Khurshid Asghar is working as an Assistant Professor of Computer Science at Department of Computer Science University of Okara, Pakistan. He earned his PhD (Computer Science) from COMSATS University Islamabad, Lahore Campus, in the field of artificial intelligence. Mr. Asghar also worked as a research associate at Cardiff School of Computer Science and Informatics, Cardiff University, UK. His current research interest includes image processing, image forensics, video forensics, machine

learning, deep learning, network security, biometrics, medical imaging and brain signals and geometric modeling.



Xianfang Sun received his Ph.D. degree in control theory and its applications from the Institute of Automation, Chinese Academy of Sciences. He is a senior lecturer at Cardiff University. His research interests include computer vision and graphics, pattern recognition and artificial intelligence, and system identification and control.



Paul L. Rosin is a Professor at the School of Computer Science & Informatics, Cardiff University. His previous posts include Brunel University, Joint Research Centre, Italy and Curtin University of Technology, Australia. His research interests include the representation, segmentation, and grouping of curves, knowledge-based vision systems, early image representations, low-level image processing, machine vision approaches to remote sensing, methods for evaluation of approximation

algorithms, medical and biological image analysis, mesh processing, non-photorealistic rendering, and the analysis of shape in art and architecture.



Mubbashar Saddique is working as a Lecturer at Department of Computer Science University of Okara, Pakistan. He completed BSc (Telecommunication Engineering) from Institute of Engineering & Technology, Lahore Campus, Pakistan. He got merit scholarship from COMSATS University Islamabad, Pakistan where he completed his MS computer science in 2010. Presently, he was a PhD Scholar at COMSATS University Islamabad, Pakistan. Mr. Saddique also worked as a research associate at

Department of Cyber Defense Graduate School of Information Security, Korea University, South Korea. Currently, he is working in video and image forensic domain. Furthermore, his research interest is in the area of image/video processing, computer vision, machine learning, data mining and networks.



Muhammad Hussain is working as a Professor at Department of Computer Science, King Saud University, Saudi Arabia. He earned his PhD from Kyushu University, Fukuoka, Japan, in 2003 in the field of Computer Graphics. He has about 21 years teaching and research experience. His current research interest includes image processing, pattern recognition, machine learning, deep learning, biometrics, medical imaging and brain signals.



Zulfiqar Habib earned his PhD degree in Computer Science in 2004 from Kagoshima University, Japan, followed by the award of postdoctoral fellowship of two years by Japan Society for the Promotion of Science (JSPS). Dr. Habib has served as the Chairman of Department of Computer Science, COMSATS University Islamabad (CUI), and currently holding the position of Professor. He is also working as the coordinating principal investigator and country representative for European Union's Horizon 2020, MSCA-RISE-2017. Dr. Habib's teaching and research interests include computer graphics, computer vision, machine learning, and robotics. Dr. Habib has achieved various awards in education and research including two Research Productivity Awards at the national level, best researcher award from CUI, and two graduate merit fellowships by Japan. Since 2009, he has been invited to give keynote lectures or tutorials in numerous national and International conferences and as the guest researcher in the universities of Germany, Turkey and UK.